Anisotropic magneto-optical effects in one-dimensional diluted magnetic semiconductors

Yukihiro Harada, Takashi Kita,* and Osamu Wada
Department of Electrical and Electronics Engineering, Faculty of Engineering, Kobe University, Rokkodai 1-1, Nada, 657-8501 Kobe, Japan

Hiroaki Ando
Department of Physics, Faculty of Science and Engineering, Konan University, Okamoto 8-9-1, Higashi-Nada, 658-8501, Kobe, Japan
(Received 6 October 2006; published 19 December 2006)

Anisotropic magnetic-field evolution of the valence-band states in ideal $Cd_{1-x}Mn_xTe$ quantum wire structures have been studied theoretically by using multiband effective-mass method. The heavy- and light-hole bands show significant mixing owing to both the one-dimensional quantum confinement and the *p-d* exchange interaction. Because of the anisotropy of the initial quantization condition determined by the one-dimensional confinement, the Zeeman diagram of the valence bands exhibits anisotropic characteristics depending on the direction of the external magnetic field. According to the magnetic-field evolution of the valence-band states, the optical transition probability shows a dramatic change in the polarization.

DOI: 10.1103/PhysRevB.74.245323 PACS number(s): 78.67.Lt, 75.50.Pp, 75.75.+a, 78.20.Ls

I. INTRODUCTION

Spin of electrons in semiconductors has been attracting increasing interest for novel spin-based functional devices.[1] Diluted magnetic semiconductors (DMS's) are expected to be a key material system, which creates magnetic properties such as ferromagnetization,[2–6] giant Zeeman splitting,[7,8] and resulting various kinds of spin-polarized phenomena[9] in semiconductors. The II-VI group DMS's such as $Cd_{1-x}Mn_xTe$ have been studied for the past few decades,[10] while the III-V DMS's have great advantages based on established reliable epitaxial growth and doping technologies. In particular, the crystal quality of Mn-containing II-VI alloys is known to be excellent and has been demonstrating various novel spin-related phenomena in semiconductors.[9,10] Here, the *sp-d* exchange interaction of spins between carriers and magnetic ions plays an important role.[9] The *s* and *p* states of the semiconductors can be controlled by the shape and size. In particular, the *p* electronic states characterizing the valence-band structures is changed significantly by both the size and dimension of heterostructures. Besides, the projection of the total angular momentum to the growth direction J_z is no longer a good quantum number even at Γ_8 in the low-dimensional heterostructures such as quantum wire (QWR) and quantum dot (QD). Thereby, the valence-band states become a mixture of the heavy- and light-hole components. The valence-band mixing effects have been confirmed by studying optical properties in the QWR (Refs. 11–15) and QD,[16,17] which realizes tunable optical performance. By doping magnetic ions into the low-dimensional heterostructures, the valence-band structure can be controlled by the *p-d* exchange interaction. Therefore, the optical properties, such as transition probability and polarization, become to be a function of magnetic field.

Low-dimensional DMS heterostructures have been expected to realize strong magneto-optical effects by utilizing the strongly confined excitonic states. In particular, it is noted that the effects sensitively depend on the magnetic field direction, because of the quantization direction in the heterostructure. For example, the Zeeman diagram of quantum wells (QW's) of DMS in the Voigt configuration shows a quite different feature from the magnetic-field dependence in the Faraday configuration.[18–21] Such anisotropic behavior depending on the magnetic field direction is caused by the hole-spin reorientation, where the heavy- and light-hole bands are mixed heavily. On the other hand, magneto-optical properties in the lower-dimensional DMS heterostructures have been investigated theoretically in $Cd_{0.97}Mn_{0.03}Te/Cd_{0.72}Mg_{0.25}Mn_{0.03}Te$ QWR's,[22,23] $Cd_{0.97}Mn_{0.03}Te$ QD's,[24] and $Cd_{1-x}Mn_xTe/Cd_{1-y}Mg_yTe$ QD's.[25] Oka *et al.* have demonstrated experimentally a large Zeeman shift in $Cd_{0.95}Mn_{0.05}Te/Cd_{0.90}Mg_{0.10}Te$ QWR's,[26] $Zn_{0.69}Cd_{0.23}Mn_{0.08}Se$ QWR's,[27] $Cd_{0.92}Mn_{0.08}Se$ QD's,[28] and $Zn_{0.69}Cd_{0.23}Mn_{0.08}Se$ QD's.[27] However, there are no reports about detailed magnetic field dependence of the valence-band states in the DMS QWR's and QD's.

Recently, we have found dramatic anisotropic magneto-optical phenomena in $(CdTe)_{0.5}(Cd_{0.75}Mn_{0.25}Te)_{0.5}$ tilted superlattices (TSL's) fabricated by the fractional monolayer growth onto a $Cd_{0.74}Mg_{0.26}Te(001)$ vicinal surface.[29] The TSL's are considered to be equivalent to $[1\bar{1}0]$-oriented QWR's lying on the (001) plane. The observed magneto photoluminescence (PL) have been found to depend on the direction of the external magnetic field in the Voigt configuration. The Zeeman shift in the magnetic field parallel to the QWR direction becomes smaller than that in the perpendicular magnetic field. Furthermore, it has been demonstrated by applying the parallel magnetic field to the QWR that the linear polarization of the QWR PL is rotated in the (001) plane. The change in the anisotropic magneto-optical properties in the QWR is significant, and needs to be clarified. In this work, we have studied theoretically the magnetic-field evolution of the valence-band structure and resultant anisotropic magneto-optical characteristics in ideal $Cd_{1-x}Mn_xTe$ QWR's.

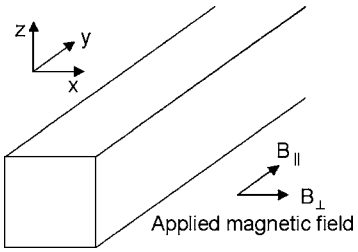

FIG. 1. Configuration of the $Cd_{1-x}Mn_xTe$ QWR structure with a rectangular cross section. The potential height of the barrier layer is assumed to be infinite. In this calculation, the incident azimuth of the linearly polarized light is along the z direction, and the external magnetic field is applied along the x ($B_\perp$) or y ($B_\parallel$) direction. x, y, and z directions are parallel to the [100], [010], and [001] directions, respectively.

II. CALCULATION MODEL AND METHOD

In this section, we describe a theoretical analysis model and method on the one-dimensional band structures and the interband optical transition probability in ideal $Cd_{1-x}Mn_xTe$ QWR's with rectangular cross section. In order to deal with the optical transitions at the fundamental band gap energy, we assume that the conduction and valence bands are decoupled, and that the effect of the spin-orbit split-off band is neglected because the spin-orbit split-off energy for the split-off band in the bulk $Cd_{1-x}Mn_xTe$ is tens of times larger than the intervalence-subband energy. Figure 1 shows the configuration used here for the $Cd_{1-x}Mn_xTe$ QWR structure. The potential height of the barrier layer is assumed to be infinite. In this calculation, the incident azimuth of the linearly polarized light is along the z direction, and the external magnetic field is applied along the x ($B_\perp$) or y ($B_\parallel$) direction. Here, x, y, and z directions are parallel to the [100], [010], and [001] directions, respectively. Treating the effect of the *sp-d* exchange interaction, we assumed that Landau quantization effect is negligible compared to the giant Zeeman splitting. We have treated the *s-d* (*p-d*) exchange interaction by adding the Heisenberg-type Hamiltonian:[30]

$$H_{s\text{-}d} = N_0\alpha x\langle \boldsymbol{S}\rangle \cdot \boldsymbol{s}, \tag{1}$$

$$H_{p\text{-}d} = \frac{1}{3}N_0\beta x\langle \boldsymbol{S}\rangle \cdot \boldsymbol{J}, \tag{2}$$

where $N_0\alpha$ ($N_0\beta$) is *s-d* (*p-d*) exchange constant, x is the molar fraction of the magnetic ions, $\langle \boldsymbol{S}\rangle$ is the average component of Mn-spin along the magnetic field direction, $\boldsymbol{s}$ is the electron spin operator, and $\boldsymbol{J}$ is the hole total angular momentum operator. The exchange constant of $Cd_{1-x}Mn_xTe$ is $N_0\alpha$ ($N_0\beta$)=0.22 (−0.88) eV.[30] The average component of the Mn-spin is expressed by a modified Brillouin function B_S,

$$\langle \boldsymbol{S}\rangle = S_0 B_S\left[\frac{Sg\mu_B|\boldsymbol{B}|}{k_B(T+T_0)}\right], \tag{3}$$

where S=5/2, g=2 for Mn. μ_B is the Bohr magneton, $|\boldsymbol{B}|$ is the absolute value of the applied magnetic field, and S_0 and T_0 are fitting parameters for the alignment of the Mn-spin by the external magnetic field, respectively.

A. Conduction band

The conduction-subband wave function $\psi_{\sigma,k}^{(m,n)}(\boldsymbol{r})$ and the corresponding subband energy $E_c^{(m,n)}(k)$ in the magnetic field are written

$$\psi_{\sigma,k}^{(m,n)}(\boldsymbol{r}) = \frac{2}{\sqrt{L_xL_z}}\sin\left(\frac{m\pi}{L_x}x\right)\sin\left(\frac{n\pi}{L_z}z\right)\exp(-ik_yy)u_\sigma^c, \tag{4}$$

$$E_c^{(m,n)}(k) = \frac{\hbar^2}{2m_e^*}\left\{\left(\frac{m\pi}{L_x}\right)^2 + \left(\frac{n\pi}{L_z}\right)^2 + k_y^2\right\} + 2\sigma H_{s\text{-}d}, \tag{5}$$

where m_e is the electron effective mass, $\sigma=\pm 1/2$, k_y is the wave vector in the y direction, and L_x and L_z are the QWR size of the x and z directions, respectively. u_σ^c are the Bloch functions at the bottom of the conduction band,

$$u_{+1/2}^c = i|s\uparrow\rangle,$$

$$u_{-1/2}^c = i|s\downarrow\rangle. \tag{6}$$

It is noted that the conduction subbands show isotropic Zeeman diagram independent of the applied magnetic field direction in this calculation model.

B. Valence band

The valence-band mixing induced by the one-dimensional quantum confinement is treated by using the multiband effective-mass method based on the four-band Luttinger-Kohn Hamiltonian H_{LK}:[31]

$$H_{LK} = \begin{pmatrix} H_{hh} & c & b & 0 \\ c^+ & H_{lh} & 0 & -b \\ b^+ & 0 & H_{lh} & c \\ 0 & -b^+ & c^+ & H_{hh} \end{pmatrix}, \tag{7}$$

where

$$H_{hh} = \frac{\hbar^2}{2m_0}[(\gamma_1+\gamma_2)(\partial_x^2 - k_y^2) + \partial_z(\gamma_1 - 2\gamma_2)\partial_z], \tag{8}$$

$$H_{lh} = \frac{\hbar^2}{2m_0}[(\gamma_1-\gamma_2)(\partial_x^2 - k_y^2) + \partial_z(\gamma_1 + 2\gamma_2)\partial_z], \tag{9}$$

$$b = -\frac{\sqrt{3}\hbar^2}{m_0}(\partial_x + k_y)\left(\frac{\gamma_3\partial_z + \partial_z\gamma_3}{2}\right), \tag{10}$$

$$c = -\frac{\sqrt{3}\hbar^2}{2m_0}\left(\frac{\gamma_2+\gamma_3}{2}\right)(\partial_x + k_y)^2. \tag{11}$$

Here, m_0 is the electron rest mass and γ's are the Luttinger parameters. The Luttinger-Kohn matrix of the QWR structure is obtained by replacing $k_x \rightarrow -i\partial_x$ and $k_z \rightarrow -i\partial_z$, and by

an appropriate unitary transformation in the original matrix.[14]

The base function set u_j^v $(j=\pm 1/2, \pm 3/2)$ for the matrix operator in Eq. (7) comprises the Bloch functions at the top of valence bands, which are expressed as

$$u_{+3/2}^v = -\frac{1}{\sqrt{2}}|(X+iY)\uparrow\rangle, \tag{12}$$

$$u_{-1/2}^v = \frac{1}{\sqrt{6}}|(X-iY)\uparrow\rangle + \sqrt{\frac{2}{3}}|Z\downarrow\rangle, \tag{13}$$

$$u_{+1/2}^v = -\frac{1}{\sqrt{6}}|(X+iY)\downarrow\rangle + \sqrt{\frac{2}{3}}|Z\uparrow\rangle, \tag{14}$$

$$u_{-3/2}^v = \frac{1}{\sqrt{2}}|(X-iY)\downarrow\rangle. \tag{15}$$

Here, we defined the heavy- and light-holes as the $j=\pm 3/2$ and $\pm 1/2$ components in the base function set u_j^v, respectively. The hole wave functions are represented by the expanded orthogonal function set,

$$\psi_k^q(\boldsymbol{r}) = \frac{2}{\sqrt{L_x L_z}} \sum_{mnj} C_{jk}^{qmn} \sin\left(\frac{m\pi}{L_x}x\right)\sin\left(\frac{n\pi}{L_z}z\right)\exp(-ik_y y)u_j^v, \tag{16}$$

where m and n are the indices of the hole envelope functions in the x and z directions, respectively. C_{jk}^{qmn} is the expansion coefficient. q is the indices of the valence subbands from the highest subband. Substituting the expanded wave function into the matrix equation,

$$(H_{\mathrm{LK}} + H_{p\text{-}d} - E_k^{vq})\psi_k^q(\boldsymbol{r}) = 0, \tag{17}$$

we get a secular equation of a $4mn \times 4mn$ matrix to be solved for the eigenenergies E_k^{vq} and the eigenvectors C_{jk}^{qmn} of each valence subband. On the other hand, the wave function distribution of the envelope components for the base function set u_j^v in the qth valence subbands can be expanded using the eigenvectors C_{jk}^{qmn} by the following equation:

$$|\langle u_j^v|\psi_k^q(\boldsymbol{r})\rangle|^2 = \frac{4}{L_x L_z}\left|\sum_{mn} C_{jk}^{qmn}\sin\left(\frac{m\pi}{L_x}x\right)\sin\left(\frac{n\pi}{L_z}z\right)\right|^2. \tag{18}$$

In this paper, we used bulk parameters of $Cd_{0.90}Mn_{0.10}Te$ (Ref. 18) and calculated eigenstates by the expanded orthogonal functions with indices m and n from 1 up to 10 in Eq. (16).

C. Interband optical transition properties

The optical transition probability between the conduction subband $c_{m,n}$ and the qth valence subband v_q is described by the squared transition matrix element,

$$|M_k^{q-(m,n)}|^2 = \sum_\sigma |\langle \psi_{\sigma,k}^{(m,n)}|\vec{\varepsilon}\cdot\vec{p}|\psi_k^q\rangle|^2 = K_k^{q-(m,n)}|\langle c|\vec{p}|v\rangle|^2, \tag{19}$$

where $|\langle c|\vec{p}|v\rangle|^2$ is the momentum matrix element for $Cd_{1-x}Mn_xTe$ bulk and $K_k^{q-(m,n)}$ is the factor of anisotropy of the optical transition probability expressed as

$$K_k^{q-(m,n)} = \frac{1}{2}(|C_{3/2,k_y}^{qmn}|^2 + |C_{-3/2,k_y}^{qmn}|^2) + \frac{1}{6}(|C_{-1/2,k_y}^{qmn}|^2 + |C_{1/2,k_y}^{qmn}|^2) \pm \frac{1}{2\sqrt{3}}(C_{3/2,k_y}^{*qmn}C_{-1/2,k_y}^{qmn} + C_{1/2,k_y}^{*qmn}C_{-3/2,k_y}^{qmn} + \text{c.c.}). \tag{20}$$

The signs + and − in the third term of Eq. (20) correspond to the polarization vector parallel and perpendicular to the QWR, respectively. The heavy- and light-hole mixing produces the polarization anisotropy of the optical transition probability as derived by the third term of Eq. (20).

III. NUMERICAL RESULTS AND DISCUSSION

A. Valence band structures in zero magnetic field

The valence subband states of the QWR structures are the mixture of the heavy- and light-hole bands due to the two-dimensional quantum confinement, and so the valence subband states strongly depend on the shape and the size of the QWR. The contribution of the heavy- and light-hole components of the valence subbands to the optical transition probability are independent of the wire size when we treat the same cross section. Here we focus on the aspect ratio (AR) dependence of the valence-band states. Figure 2(a) shows the AR dependence of the heavy- and light-hole components of the highest valence subband at Γ_8. Here, the AR of the QWR cross section is denoted by L_z/L_x. The highest valence subband is mainly composed of $(m,n,j)=(1,1,\pm 1/2)$ and $(1,1,\pm 3/2)$ components in all the AR's because of quite small contributions of the higher indices of the hole envelope functions. The highest valence subband in the smaller AR consists of the heavy-hole component dominantly. With increasing the AR, the light-hole component increases, then crosses over the heavy-hole component at the AR of 1.4. Figure 2(b) shows the AR dependence of the linear polarization of the optical transition probability between the lowest conduction and the highest valence subbands at Γ_8. The polarization is defined as $P=(I_\parallel - I_\perp)/(I_\parallel + I_\perp)$, where $I_\parallel$ and $I_\perp$ are the optical transition components of the parallel and perpendicular to the QWR, respectively. Since the lowest conduction subband consists of $(m,n)=(1,1)$ component, only $(m,n,j)=(1,1,\pm 1/2)$ and $(1,1,\pm 3/2)$ components of the highest valence subband contribute to the optical transition. When the AR is small, in other words, the lateral confinement is weak, the transition is almost isotropic, which is like a QW. With increasing the AR, the polarization is increased remarkably. The strong lateral confinement in the high AR

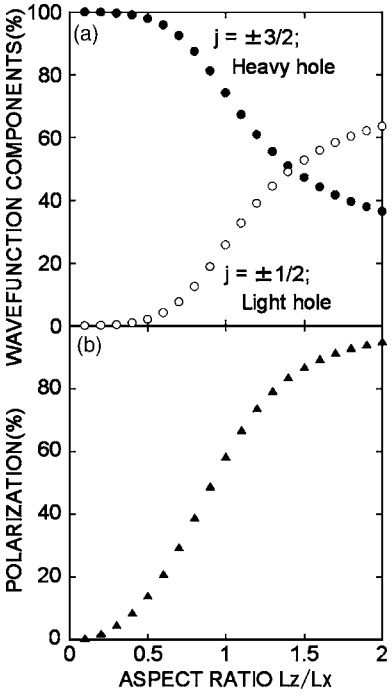

FIG. 2. (a) AR dependence of the heavy- and light-hole components of the highest valence subband at Γ_8. Here, the AR of the QWR cross section is denoted by L_z/L_x. (b) AR dependence of the linear polarization of the optical transition probability between the lowest conduction and the highest valence subbands at Γ_8. The polarization is defined as $P=(I_{\parallel}-I_{\perp})/(I_{\parallel}+I_{\perp})$, where $I_{\parallel}$ and $I_{\perp}$ are the optical transition components of the parallel and perpendicular to the QWR, respectively.

results in the strong heavy- and light-hole mixing and causes the preferential polarization along the wire direction. Next, we focus on the AR of 0.77, 1.00, and 1.43 in order to understand effects of the QWR shape on the magneto-optical properties.

B. Anisotropic Zeeman effects and transition polarization in Voigt configuration

Figure 3 summarizes Zeeman diagrams of the valence subbands at Γ_8 for $Cd_{0.90}Mn_{0.10}Te$ QWR's with cross-sectional areas of (a) 13×10 nm^2, (b) 10×10 nm^2, and (c) 7×10 nm^2. The top and bottom display the results in the magnetic field applied perpendicular and parallel to the QWR direction, respectively. The Zeeman diagram shows significant anisotropy depending on the applied field direction. It is noted that with increasing the AR the anisotropy becomes remarkable. The Zeeman shift in the parallel magnetic field is found to be suppressed, which results when the in-plane quantum confinement tends to prevent the hole spin from rotating into the external field direction. Furthermore, a valence-band crossing is clearly observed. That is a direct evidence of the hole-spin reorientation causing the valence-band mixing. In zero magnetic field, the first and the third valence subbands are mainly mixture of $(m,n,j)=(1,1,\pm1/2)$ and $(1,1,\pm3/2)$. On the other hand, the second subband consists of $(m,n,j)=(1,2,\pm1/2)$, $(2,1,\pm1/2)$, $(1,2,\pm3/2)$, and $(2,1,\pm3/2)$ components.[32] An anticrossing behavior between the first and the third subbands is observed in Figs. 3(a) and 3(c) owing to a repulsive interaction produced by the off-diagonal element of the Luttinger-Kohn Hamiltonian. The wave functions exchange their characters where the third subband comes close to the first subband. On the other hand, in Fig. 3(b) of the isotropic shape QWR, the third subband intersects with the first subband because the wave functions are orthogonal at $L_x=L_z$.

In order to study wave function distributions in the QWR in the magnetic field, we have calculated the envelope components in the isotropic shape QWR. The cross section is 10×10 nm^2. Figure 4 shows cross-sectional images of the highest valence subband wave function of the envelope components obtained by Eq. (18). Figures 4(a), 4(b), and 4(c) are results in the zero-magnetic field, the perpendicular magnetic field, and the parallel magnetic field, respectively. Here, the

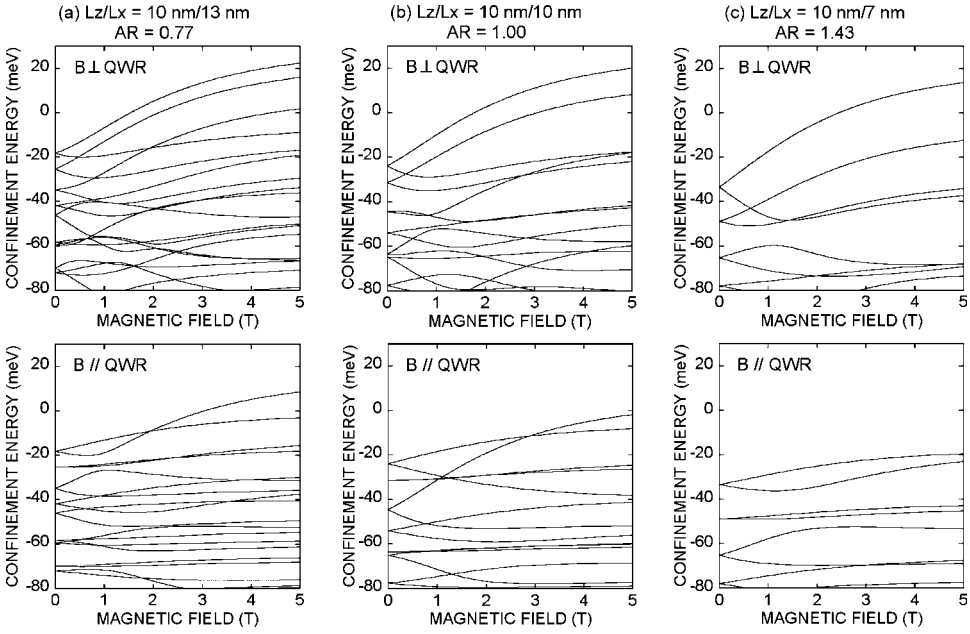

FIG. 3. Magnetic field dependence of the Zeeman diagram of the valence subbands at Γ_8 for $Cd_{0.90}Mn_{0.10}Te$ QWR's with cross-sectional areas of (a) 13×10 nm^2, (b) 10×10 nm^2, and (c) 7×10 nm^2. The top and bottom display the results in the magnetic field applied perpendicular and parallel to the QWR direction, respectively.

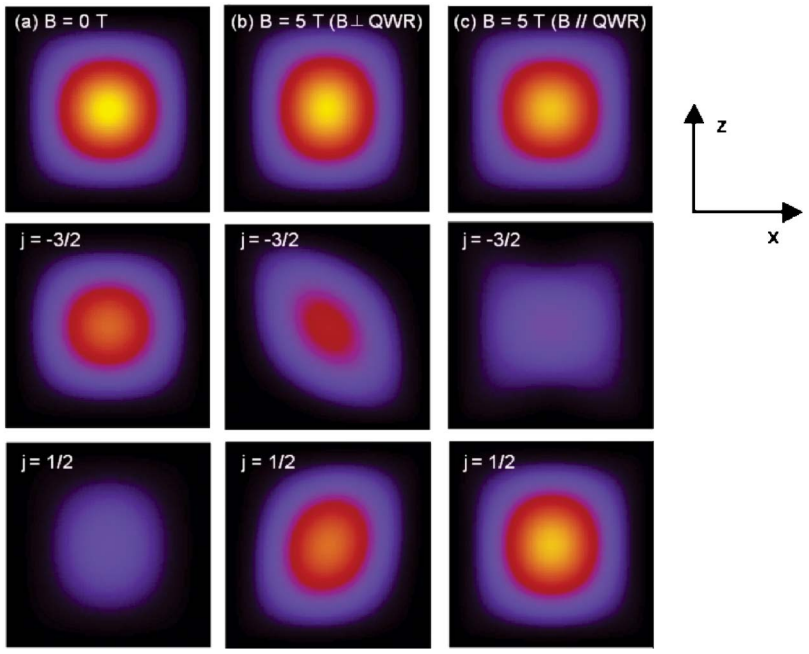

FIG. 4. (Color online) Cross-sectional images of the highest valence subband wave function of the envelope components in the QWR with cross-sectional area of 10×10 nm^2. (a), (b), and (c) are results in the zero-magnetic field, the perpendicular magnetic field, and the parallel magnetic field, respectively. Here, the magnitude of the applied magnetic field is 5 T. On the other hand, the top, middle, and bottom figures display the total wave function, the heavy-hole component ($j=-3/2$), and the light-hole component ($j=1/2$), respectively.

magnitude of the applied magnetic field is 5 T. On the other hand, the top, middle, and bottom figures display the total wave function, the heavy-hole component ($j=-3/2$), and the light-hole component ($j=1/2$), respectively. In the zero-magnetic field, as indicated in Fig. 2(a), the heavy-hole component is dominant. When applying the magnetic field, the *p-d* exchange interaction mixes the heavy- and light-hole states. Thereby, the light-hole component becomes remarkable. In the parallel magnetic field, the hole spin is reoriented, and the valence-band character is replaced as appeared in Fig. 3. That causes the substantial light-hole character in Fig. 4(c). In the perpendicular magnetic field, the total wave function is compressed along the magnetic field direction. The anisotropic shape of the heavy-hole component ($j=-3/2$) and the light-hole component ($j=1/2$) in the perpendicular magnetic field is caused by the *p-d* exchange interaction inclining the quantization direction to the x direction for the $j=-3/2$ component and to the $-x$ direction for the $j=1/2$ component, respectively.

Next, we discuss the magnetic field induced energy shift, i.e., the Zeeman shift. The calculated Zeeman shift of the highest valence subband in the $Cd_{0.90}Mn_{0.10}Te$ QWR's with cross-sectional areas of (a) 13×10 nm^2, (b) 10×10 nm^2, and (c) 7×10 nm^2 are shown in Fig. 5. The solid and dashed lines represent results in the magnetic field applied perpendicular and parallel to the QWR, respectively. The Zeeman shift in the perpendicular magnetic field becomes larger than that in the parallel magnetic field, which is enhanced with increasing the AR. This is due to the strong quantization perpendicular to the QWR direction. On the other hand, in the parallel magnetic field, the shift is suppressed because of the orthogonal configuration between the initial quantization and the external field, where the hole spin is reoriented. We note a cusp structure as indicated by the arrow. The cusp structure results from the valence-band crossing as revealed in Fig. 3. Before crossing the bands, the highest valence subband has the heavy-hole character, while the character is changed into the light-hole after that. The cusp shifts toward the higher magnetic field with increasing the AR, because of the stronger lateral quantization in the higher AR QWR.

Figure 6 shows the magnetic field dependence of the linear polarization transition probability at Γ_8 of the $Cd_{0.90}Mn_{0.10}Te$ QWR's with the cross-sectional areas of (a) 13×10 nm^2, (b) 10×10 nm^2, and (c) 7×10 nm^2. As depicted in the inset of Fig. 6(a), closed circles represent the transition from the highest valence subband in the magnetic field perpendicular to the QWR, and open squares and triangles indicate results of the transition from the highest and the second-highest valence subbands in the parallel magnetic field, respectively. The polarization sensitively depends on the magnetic field direction and the magnitude. As plotted by the closed circles in the perpendicular magnetic field, the polarization increases monotonically. This indicates that the quantization along the perpendicular direction to the QWR is strengthened by the magnetic field. On the other hand, in the parallel magnetic field, we found an abrupt change in the polarization as shown in Figs. 6(a) and 6(b). With increasing magnetic field in this configuration, the heavy-hole dominant subband polarized parallel to the QWR is the topmost level up to ~2 T. And then, as shown in the inset of Fig. 3, the light-hole dominant state rises and intersects with the topmost subband near 2 T. Since the character of the topmost level is changed from the heavy-hole dominant state into the light-hole dominant state, the polarization shows such sudden jump. As discussed here, the valence-band crossing plays a key role in the anisotropic Zeeman shift and optical polarization depending on the magnetic-field direction.

IV. CONCLUSION

We have studied theoretically anisotropic magnetic-field evolution of the valence-band states in $Cd_{1-x}Mn_xTe$ QWR structures by using multiband effective-mass method. The heavy- and light-hole bands show significant mixing owing

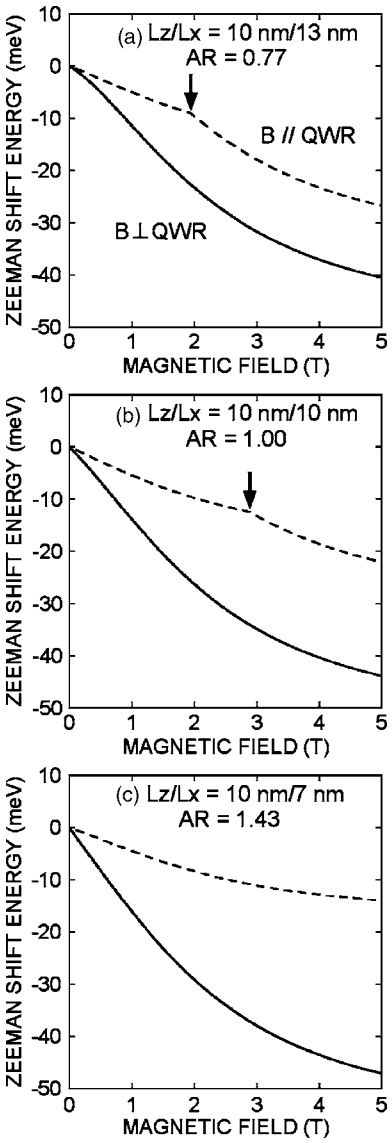

FIG. 5. Magnetic field dependence of the Zeeman shift of the highest valence subband in the $Cd_{0.90}Mn_{0.10}Te$ QWR's with cross-sectional areas of (a) 13×10 nm^2, (b) 10×10 nm^2, and (c) 7×10 nm^2. The solid and dashed lines represent results in the magnetic field applied perpendicular and parallel to the QWR, respectively.

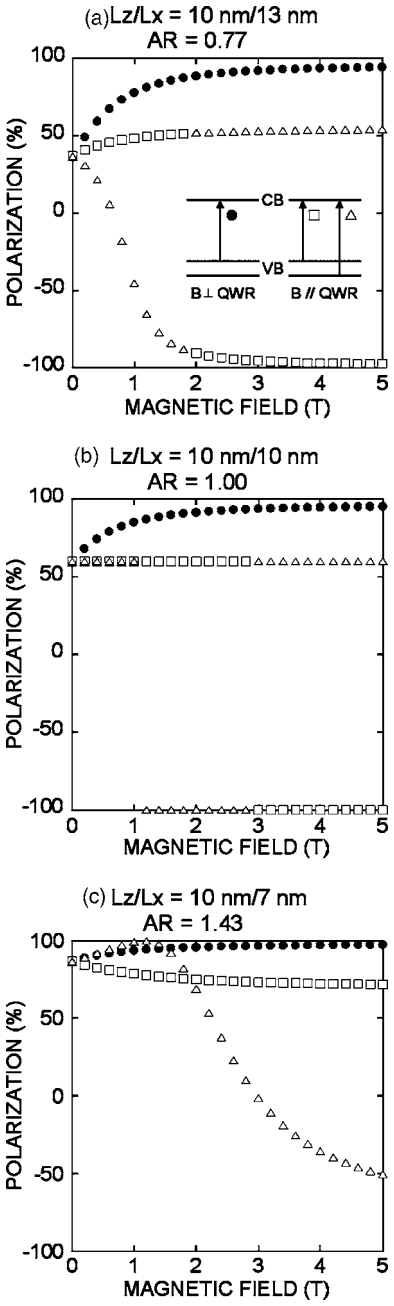

FIG. 6. Magnetic field dependence of the linear polarization transition probability at Γ_8 of the $Cd_{0.90}Mn_{0.10}Te$ QWR's with the cross-sectional areas of (a) 13×10 nm^2, (b) 10×10 nm^2, and (c) 7×10 nm^2. As depicted in the inset of (a), closed circles represent the transition from the highest valence subband in the magnetic field perpendicular to the QWR, and open squares and triangles indicate results of the transition from the highest and the second-highest valence subbands in the parallel magnetic field, respectively.

to both the one-dimensional quantum confinement and the *p-d* exchange interaction. Because of the anisotropy of the initial quantization condition determined by the one-dimensional confinement, the Zeeman diagram of the valence bands exhibits anisotropic characteristics depending on the direction of the external magnetic field. The Zeeman shift in the perpendicular magnetic field becomes larger than that in the parallel magnetic field, which is enhanced with increasing the AR of the QWR cross section because of the strong quantization perpendicular to the QWR direction. According to the magnetic field evolution of the valence-band states, the optical transition probability shows a dramatic change in the polarization. In the parallel magnetic field, the polarization shows an abrupt change in the small AR QWR's, while in the perpendicular magnetic field, the polarization increase monotonically. We found that the valence-band crossing caused by the hole-spin reorientation plays a key role in the anisotropic Zeeman shift and optical polarization depending on the magnetic-field direction.

*Electronic address: kita@eedept.kobe-u.ac.jp

[1] S. A. Wolf, D. D. Awschalom, R. A. Buhrman, J. M. Daughton, S. von Molnár, M. L. Roukes, A. Y. Chtchelkanova, and D. M. Treger, Science **294**, 1488 (2001).
[2] H. Ohno, H. Munekata, T. Penney, S. von Molnár, and L. L. Chang, Phys. Rev. Lett. **68**, 2664 (1992).
[3] H. Ohno, A. Shen, F. Matsukura, A. Oiwa, A. Endo, S. Katsumoto, and Y. Iye, Appl. Phys. Lett. **69**, 363 (1996).
[4] S. Koshihara, A. Oiwa, M. Hirasawa, S. Katsumoto, Y. Iye, C. Urano, H. Takagi, and H. Munekata, Phys. Rev. Lett. **78**, 4617 (1997).
[5] H. Ohno, Science **281**, 951 (1998).
[6] H. Saito, V. Zayets, S. Yamagata, and K. Ando, Phys. Rev. Lett. **90**, 207202 (2003).
[7] R. L. Aggarwal, S. N. Jasperson, P. Becla, and R. R. Galazka, Phys. Rev. B **32**, 5132 (1985).
[8] R. L. Aggarwal, S. N. Jasperson, P. Becla, and J. K. Furdyna, Phys. Rev. B **34**, 5894 (1986).
[9] J. K. Furdyna, J. Appl. Phys. **64**, R29 (1988).
[10] S. Takeyama, in *Optical Properties of Low-Dimensional Materials*, edited by T. Ogawa and Y. Kanemitsu (World Scientific, USA, 1998), Vol. 2.
[11] D. S. Citrin and Y.-C. Chang, Phys. Rev. B **43**, 11703 (1991).
[12] P. C. Sercel and K. J. Vahala, Phys. Rev. B **44**, 5681 (1991).
[13] C. Pryor, Phys. Rev. B **44**, 12912 (1991).
[14] U. Bockelmann and G. Bastard, Phys. Rev. B **45**, 1688 (1992).
[15] F. Vouilloz, D. Y. Oberli, M.-A. Dupertuis, A. Gustafsson, F. Reinhardt, and E. Kapon, Phys. Rev. B **57**, 12378 (1998).
[16] J. L. Pan, Phys. Rev. B **46**, 4009 (1992).
[17] T. Saito, T. Nakaoka, T. Kakitsuka, Y. Yoshikuni, and Y. Arakawa, Physica E (Amsterdam) **26**, 217 (2005).
[18] T. Z. Kachlishvili, Solid State Commun. **80**, 283 (1991).
[19] P. Peyla, A. Wasiela, Y. Merle d'Aubigné, D. E. Ashenford, and B. Lunn, Phys. Rev. B **47**, 3783 (1993).
[20] B. Kuhn-Heinrich, W. Ossau, E. Bangert, A. Waag, and G. Landwehr, Solid State Commun. **91**, 413 (1994).
[21] D. Suisky, W. Heimbrodt, C. Santos, F. Neugebauer, M. Happ, B. Lunn, J. E. Nicholls, and D. E. Ashenford, Phys. Rev. B **58**, 3969 (1998).
[22] F. V. Kyrychenko and J. Kossut, Phys. Rev. B **61**, 4449 (2000).
[23] F. V. Kyrychenko and J. Kossut, Physica E (Amsterdam) **10**, 378 (2001).
[24] F. V. Kyrychenko and J. Kossut, Phys. Rev. B **70**, 205317 (2004).
[25] K. Chang, S. S. Li, J. B. Xia, and F. M. Peeters, Phys. Rev. B **69**, 235203 (2004).
[26] Z. H. Chen, M. C. Debnath, K. Shibata, T. Saitou, T. Sato, and Y. Oka, J. Appl. Phys. **89**, 6701 (2001).
[27] Y. Oka, K. Kayanuma, S. Shirotori, A. Murayama, I. Souma, and Z. Chen, J. Lumin. **100**, 175 (2002).
[28] N. Takahashi, K. Takabayashi, I. Souma, J. Shen, and Y. Oka, J. Appl. Phys. **87**, 6469 (2000).
[29] S. Nagahara, T. Kita, O. Wada, L. Marsal, and H. Mariette, Phys. Rev. B **69**, 233308 (2004).
[30] J. A. Gaj, R. Planel, and G. Fishman, Solid State Commun. **29**, 435 (1979).
[31] J. M. Luttinger, Phys. Rev. **102**, 1030 (1956).
[32] H. Ando, S. Nojima, and H. Kanbe, J. Appl. Phys. **74**, 6383 (1993).